Author(s): Moilanen, Jani; Mansikkamäki, Akseli; Lahtinen, Manu; Guo, Fu-Sheng; Kalenius, Elina; Layfield, Richard A.; Chibotaru, Liviu F.

Title: Thermal expansion and magnetic properties of benzoquinone-bridged dinuclear rare-earth complexes

Year: 2017

Version: Accepted version (Final draft)

Please cite the original version:

Moilanen, J., Mansikkamäki, A., Lahtinen, M., Guo, F.-S., Kalenius, E., Layfield, R. A., & Chibotaru, L. F. (2017). Thermal expansion and magnetic properties of benzoquinone-bridged dinuclear rare-earth complexes. Dalton Transactions, 46(39), 13582-13589. https://doi.org/10.1039/C7DT02565C

Thermal expansion and magnetic properties of benzoquinone-bridged dinuclear rare-earth complexes

Jani O. Moilanen,*[a] Akseli Mansikkamäki,[a] Manu Lahtinen,[a] Fu-Sheng Guo,[b] Elina Kalenius,[a] Richard A. Layfield,[b] and Liviu F. Chibotaru[c]

The synthesis and structural characterization of two benzoquinone-bridged dinuclear rare-earth complexes [BQ(MCl_2·THF_3)$_2$] (BQ = 2,5-bisoxide-1,4-benzoquinone; M = Y (**1**), Dy (**2**)) are described. Of these reported metal complexes, the dysprosium analogue **2** is the first discrete bridged dinuclear lanthanide complex in which both metal centres reside in pentagonal bipyramidal environments. Interestingly, both complexes undergo significant thermal expansion upon heating from 120 K to 293 K as illustrated by single-crystal X-ray and powder diffraction experiments. AC magnetic susceptibility measurements reveal that **2** does not show the slow relation of magnetization in zero dc field. The absent of single-molecule behaviour in **2** arises from the rotation of the principal magnetic axis as compared to the pseudo-C_5 axis of the pentagonal bipyramidal environment as suggested by *ab initio* calculations. The cyclic voltammetry and chemical reduction experiments demonstrated that complexes **1** and **2** can be reduced to radical species containing [$BQ^{3\bullet-}$]. This study establishes efficient synthetic strategy to make bridged redox-active multinuclear lanthanide complexes with a pentagonal bipyramidal coordination environment that are potential precursors for single-molecule magnets.

Introduction

The redox active ligand 2,5-dihydroxy-1,4-benzoquinone (DHBQ) can function as a bridging unit between two metal centres.[1] Its ability to bind transition metals has been utilized to synthesize a plethora of dinuclear transition metal complexes,[1,2] magnetically ordered metal-organic frameworks[3] and cage complexes that are potential anticancer agents.[4] In contrast to the rich transition metal chemistry of DHBQ, the rare-earth chemistry of DHBQ is less developed. Only a couple of the reported structures are discrete dinuclear complexes and all others are coordination polymers.[5,6] The lack of discrete dinuclear rare earth complexes of DHBQ can be partly explained by the fact that most of the previous studies have focused on the development of extended coordination frameworks suitable for solid oxide fuel cells, gas hydrates and three-dimensional magnetic materials.[5b,6e-g] The redox activity of DHBQ, and its two coordinating pockets with hard donor atoms provide an excellent opportunity to synthesize bridged dinuclear rare-earth complexes and scope their redox properties.

Previous studies focused on dinuclear lanthanide complexes with pentagonal bipyramidal symmetry around the lanthanide centres have shown that these complexes possess intriguing magnetic properties, such as single-molecule magnetism.[7] In all four such complexes the metal centres are bridged by two Schiff base ligands. Also, carboxylate groups or chloride ions have been used as a bridging unit in three reported 1D-chain lanthanide complexes that show single-molecule magnetic behaviour and feature pentagonal bipyramidal environments around the lanthanide centres.[8] Thus, the range of ligands to bridge between pentagonal bipyramidal lanthanide centres is still rather limited. Particularly, interesting bridging units are redox-active ligands because they serve as building blocks for the radical bridged complexes. Indeed, the redox-active ligands have been used to synthesize diamagnetic and radical bridged dinuclear lanthanide complexes that show single-molecule magnet behaviour.[9] However, to the best of our knowledge, no dinuclear lanthanide complex with local pseudo-D_{5h} coordination environments around the lanthanide ions incorporating a single bridging redox-active ligand has been previously reported.

Herein, we report the synthesis, structural characterization, redox and magnetic properties of two new benzoquinone-bridged dinuclear rare-earth complexes [BQ(MCl_2·THF_3)$_2$] (M = Y (**1**), Dy (**2**)) of which the dysprosium analogue represents the first example of pentagonal bipyramidal dinuclear lanthanide complex containing one redox active ligand as a bridging unit.

Experimental section

General considerations

The synthesis and manipulation of all compounds was carried out employing standard Schlenk and glovebox techniques in an inert atmosphere of argon. Solvents were dried by refluxing them either over CaH_2 (dichloromethane, bromobenzene) or $CaCl_2$ (chloroform) or sodium without (hexanes, toluene) and with benzophenone (tetrahydrofuran, dimethoxyethane) at least three days. Solvents were then distilled, degassed and stored over activated 4 Å molecular sieves. Acetonitrile was dried by distilling it first over P_2O_5 and then refluxing it over CaH_2 at least three days before being distilled, degassed and stored over activated 3 Å molecular sieves. Trimethylsilyl chloride, triethylamine and tetrakis(dimethylamino)ethylene

(TDAE) were distilled prior to use. Anhydrous MCl_3 (RE = Y and Dy) (Strem), tetrabutylammonium hexafluorophosphate (Sigma-Aldrich) and 2,5-dihydroxy-1,4-benzoquinone (Sigma-Aldrich) were used as received. THF-d8 was degassed and refluxed over sodium for two days after which it was vacuum transferred into an ampoule and stored in the glovebox.

Single crystal X-ray crystallography and powder diffraction

The single crystals of **1**-**3** were measured with Agilent Technologies SuperNova diffractometer equipped with a multilayer optics monochromatic dual source (Cu and Mo) Atlas detector using CuKα (λ = 1.5418 Å) radiation at 120 K and 293 K. CrysalisPro was used for data acquisition, reduction and analytical face-index absorption correction.[10] the crystal structures were solved by the SHELXS[11] program using direct methods and refined by the SHELXL[12] program employing least squares minimization. Olex[2] program was used throughout the solving and refining procedures.[13]

Powder diffraction data of complexes **1** and **2** were measured with PANalytical X´Pert PRO MPD diffractometer in Bragg–Brentano geometry and Johansson monochromator to produce pure CuKα1 radiation (1.5406 Å; 45kV, 40mA). Each sample was prepared in glove box between two Kapton foils to protect the sample from air and atmospheric moisture. The data was recorded from a spinning sample by X´Celerator detector using continuous scanning mode in 2θ range of 6–70° with a step size of 0.017° and counting times of 60 s per step. The diffraction data were analysed using program PANalytical HighScore Plus v. 4.5.

EPR

The solid state X-band EPR spectrum of $\mathbf{1}^{\bullet-}$ was acquired on Magnettech MiniScope MS 200 spectrometer at 293 K using following parameters: ν = 9.3905 GHz, centre field = 334.964 mT, spectrum width = 100 mT, modulation amplitude = 2 mT and microwave attenuation = 30 dB. No solution state EPR spectrum was recorded for $\mathbf{1}^{\bullet-}$ due to its insolubility to tested organic solvents (acetonitrile, bromobenzene, chloroform, dichloromethane, dimethoxyethane, hexanes, tetrahydrofuran and toluene).

Cyclic voltammetry

Cyclic voltammetry measurements were carried out utilizing a Gamry Reference 600 potentiostat. Potentials were scanned with respect to the quasi-reference electrode in a single compartment cell fitted with Pt wire electrodes and referenced to the Fc/Fc^+ couple of ferrocene at 0.547 V vs SCE. All measurements were made under argon atmosphere using the scan rate 200 mV s^{-1} in freshly distilled and degassed THF which was 0.1 M in $[(n\text{-}Bu)_4N]^+[PF_6]^-$ supporting electrolyte at 293 K. No precise molarity of analytes (**1** and **2**) could be determined due to their poor solubility to THF.

Magnetic measurements

Magnetic experiments were performed on a Quantum Design MPMS-XL SQUID magnetometer equipped with a 7 T magnet. Variable-temperature magnetic susceptibility was measured with an external magnetic field of 10000 Oe in the temperature range of 2–300 K and the frequency dependent ac susceptibility was measured with an oscillating field of 1.55 Oe. Finely ground microcrystalline powders of samples were immobilized in eicosane matrix inside a NMR tube sealed by flame torch

NMR, IR, ICP, EA and mass spectrometry

^1H NMR and ^{13}C NMR spectra were measured on a Bruker Avance III 300 MHz and Bruker Avance DRX 500 MHz NMR spectrometers. FTIR spectra were acquired on a Bruker ALPHA platinum single reflection diamond ATR-FTIR spectrometer. ICP atomic emission spectroscopy was carried out by Perkin Elmer Optima 8300 DV ICP spectrometer and elemental analyses were performed at Elementar Vario EL III elemental analyzer.

ESI-MS experiments for complexes **1** and **2** were performed on ABSciex QSTAR Elite ESI-Q-TOF mass spectrometer equipped with an API 200 TurboIonSpray ESI source from ABSciex (former MDS Sciex) in Concord, Ontario (Canada). The sample solutions were prepared in dry THF or THF/MeCN. The samples were injected into the ESI source with a flow rate of 5 µl/min. The parameters were optimized to get maximum abundance of the ions under study. Room-temperature nitrogen was used for nebulization. The measurements and data handling were accomplished with Analyst® QS 2.0 Software. Mass spectra were externally calibrated by ESI Tuning mix (Agilent Technologies). The compositions of the ions were verified by comparing experimental *m/z* values and isotopic patterns with the theoretical ones.

Computational details

The multireference *ab initio* calculations on **2** were performed using the standard CASSCF/SO-RASSI methodology as implemented in the Molcas quantum chemistry code version 8.2.[14] The geometry of **2** was extracted from the crystal structure and used without any further optimization. Two separate calculations were carried out were the other Dy ion was replaced by an Y ion. Roos' ANO-RCC basis sets were employed throughout.[15] A VTZP quality basis set corresponding to a [9s8p6d4f3g2h] contraction was used for the Dy ions and VDZP quality basis sets corresponding to [2s1p], [3s2p1d], [3s2p1d], [4s3p1d], and [6s5p3d1f] contractions for H, C, O, Cl, and Y, respectively, were used for the other atoms. Scalar relativistic effects were treated using the exact two component (X2C) transformation.[16] State-averaged CASSCF calculations[17] correlating all nine 4f electrons in the seven 4f orbitals was performed. All 21 sextet, 224 quartet and 490 doublet roots were solved. The spin-free states obtained as solutions to the CASSCF calculations were than mixed by spin-orbit coupling using the restricted active space state interaction (SO-RASSI) method.[18] All spin sextets, 128 spin quartets and 130 spin doublets corresponding to an energy cut-off of 50,000 cm^{-1} were included in the SO-RASSI procedure. The local magnetic

properties (**g** tensor, crystal field parameters and transition magnetic moments) were then extracted from the SO-RASSI wave functions using the SINGLE_ANISO routine.[19] The exchange and dipolar interactions between the Dy ion were calculated with the POLY_ANISO routine.[20] The sixteen lowest states corresponding to the crystal-field split states of the $^6H_{15/2}$ multiplet were taken into account in the exact diagonalization of the exchange Hamiltonian. The exchange interaction was modelled using the Lines model[21] and the exchange parameter was determined by fitting the calculated susceptibility to the experimental data by scanning the exchange parameter with 0.001 cm^{-1} increments.

Synthesis of studied systems

Synthesis of 2,5-bis[(trimethylsilyl)oxy]-2,5-cyclohexadiene-1,4-dione, 3. Et_3N (4.3 g, 42.8 mmol) in THF (8 ml) was added dropwise to the brown solution of 2,5-dihydroxy-1,4-benzoquinone (2.1 g, 15.0 mmol) in THF (30 ml). The solution was stirred a hour at the ambient temperature during which a dark red precipitate formed. The precipitate was dissolved in hot THF and the solution was filtered hot. The storage of the solution at -20° afforded red crystals. Crystals were isolated by filtration and washed with hexanes (2 × 10 ml) to afford [2,5-bisoxide-1,4-benzoquinone][Et_3NH]$_2$ in yield of 4.7 g that was used in the next step without further characterization or purification.

Trimethylsilyl chloride (1.56 ml, 12.3 mmol) was slowly added to the suspension of [2,5-bisoxide-1,4-benzoquinone][Et_3NH]$_2$ (2.0 g, 5.8 mmol) in Et_2O (40 ml). The reaction gave immediately a yellow solution and white precipitate. The solution was filtered and the remaining white residue was washed with Et_2O (2 × 5ml). The combined filtrates were evaporated to dryness to give a yellow solid. The solid was dissolved in hot hexanes, filtered hot and stored in the fridge (-20°) overnight to afford 2,5-bis[(trimethylsilyl)oxy]-2,5-cyclohexadiene-1,4-dione as yellow crystals. Yield: 1.33 g (80%). EA analysis ($C_{12}H_{20}O_4Si_2$): calc.: C: 50.67; H: 7.09; found C: 50.14; H: 7.13. ^{1}H NMR (300 MHz, THF-d8, 300 K, δ/ppm) = 0.28 (s, 18H, TMS), 5.96 (s, 2H, Ar-H), 5.24. ^{13}C NMR (75 MHz, THF-d8, 300 K, δ/ppm) = 0.85, 113.24, 157.72, 184.80. IR (ν/cm^{-1}): 2961 (w), 1655 (m), 1585 (s), 1408 (w), 1368 (m), 1254 (m), 1194 (s), 901 (m), 830 (s), 787 (m), 752 (s), 693 (m), 641 (m), 554 (m).

Synthesis of [BQ(YCl_2·THF_3)$_2$], 1. The suspension of 2,5-bis[(trimethylsilyl)oxy]-2,5-cyclohexadiene-1,4-dione (400 mg, 1.4 mmol) and YCl_3 (540 mg, 2.8 mmol) in THF (35 ml) was stirred 1 hour at 55°C. Temperature was increased to 66°C and the stirring was continued 1.5 hours. The mixture was filtered hot. The remaining red residues was washed with hexanes (2 × 10 ml) and dried under vacuum to afford **1** as a red microcrystalline solid. Yield: 851 mg (68 %). EA analysis ($C_{30}H_{50}Cl_4O_{10}Y_2$): calc.: C: 40.47, H: 5.66; found C: 40.10; H: 5.34. ^{1}H NMR (300 MHz, THF-d8, 300 K, δ/ppm) = 1.78 (m, THF), 3.62 (m, THF), 5.24 (s, 2H, BQ). ^{13}C NMR (125 MHz, THF-d8, 300 K, δ/ppm) = 98.82, 184.88. ESI-Q-TOF-MS calc. for [BQ(YCl·THF_2)$_2$]$^{2+}$ ($C_{22}H_{34}O_8Cl_2Y_2$)$^{2+}$: *m/z* 336.9868; found: *m/z* 336.9858. IR (ν/cm^{-1}): 2980 (w), 2953 (w), 2886 (w), 1545 (s), 1399 (m), 1379 (m), 1286 (w), 1273 (w), 1254 (m), 1018 (m), 915 (w), 867 (m), 816 (m), 770 (w), 673 (w), 504 (w), 467 (m).

Synthesis of [BQ($DyCl_2$·THF_3)$_2$], 2. **2** was synthesized using the same synthetic procedure as for **1** employing 2,5-bis[(trimethylsilyl)oxy]-2,5-cyclohexadiene-1,4-dione (200 mg, 0.7 mmol), $DyCl_3$ (369 mg, 1.37 mmol) and THF (20 ml). Yield: 491 mg (68 %). EA analysis ($C_{30}H_{50}Cl_4O_{10}Dy_2$): calc.: C: 34.73, H: 4.86; found C: 34.28; H: 4.66. ESI-Q-TOF-MS calc. for [BQ(DyCl·THF_2)$_2$]$^{2+}$ ($C_{22}H_{34}O_8Cl_2Dy_2$)$^{2+}$: *m/z* 411.0087; found: *m/z* 411.0336. IR (ν/cm^{-1}): 2980 (w), 2950 (w), 2886 (w), 1543 (s), 1399 (m), 1379 (m), 1295 (w), 1254 (m), 1018 (m), 916 (w), 867 (m), 816 (m), 770 (w), 673 (w), 504 (w), 467 (m).

Doped sample Dy@1. The doped sample was obtained by reacting 2,5-bis[(trimethylsilyl)oxy]-2,5-cyclohexadiene-1,4-dione (202 mg, 0.71 mmol), YCl_3 (258 mg, 1.32 mmol) and $DyCl_3$ (19 mg, 0.07 mmol) in THF (35 ml) and following the same synthetic procedure as for **1**. The purity of doped sample was ensured by powder diffraction and IR experiments (Figure S13 and Figure S12). The accurate dysprosium/yttrium ratio was determined by ICP atomic emission spectroscopy to be 5.1 ± 0.2 %.

Chemical reduction of 1. The red suspension of **1** (100 mg, 0.11 mmol) and TDAE (22 mg, 0.11 mmol) was stirred in THF (4 ml) overnight during which a green precipitate formed. The green mixture was filtered and the remaining residue was washed with hexanes (2 × 3 ml) to yield a green solid as 56 mg yield. The green solid was characterized by ATR-IR and EPR spectrometers to contain radical species (Figure S5 and Figure S6). IR (ν/cm^{-1}): 2980 (w), 2880 (w), 1656 (w), 1530 (m), 1468 (m), 1397 (w), 1374 (w), 1250 (w), 1205 (w), 1168 (w), 1020 (w), 875 (m), 773 (w), 497 (w), 454 (w).

Chemical reduction of 2. The red suspension of **2** (80 mg, 0.08 mmol) and TDAE (28 mg, 0.14 mmol) was stirred in THF (4 ml) overnight during which a green precipitate formed. The green mixture was filtered and the remaining residue was washed with hexanes (2 × 3 ml) to yield a green solid as 32 mg yield. The green solid was characterized by ATR-IR to contain radical species (Figure S7). IR (ν/cm^{-1}): 2980 (w), 2890 (w), 1657 (w), 1542 (m), 1466 (m), 1399 (w), 1378 (w), 1255 (w), 1208 (w), 1167 (w), 1019 (w), 868 (m), 817 (w), 771 (w), 673 (w), 502 (w), 467 (w).

Results and discussion

To obtain targeted complexes [BQ(MCl_3·THF_3)$_2$] (M = Y (**1**), Dy (**2**), BQ = 2,5-bisoxide-1,4-benzoquinone) we reacted two equivalents of anhydrous MCl_3 with 2,5-bis[(trimethylsilyl)oxy]-2,5-cyclohexadiene-1,4-dione **3** in hot THF (Scheme 1). The reaction yielded the dinuclear bridged complexes **1** and **2** as analytically pure red crystalline solids that are sparingly soluble in THF and insoluble in other common organic solvents.

Complexes, **1** and **2** crystallize in the *P21/n* space group with the crystallographic 2-fold rotation axis passing through the centre of the BQ ligand. In **2**, the symmetry-related seven-coordinate Dy^{3+} ions occupy pentagonal bipyramidal environments with a nearly linear Cl1-Dy1-Cl2 angle 175.87(8)° (Figure 1, Figure S1 and Table S1). The O-Dy-Cl angles vary from 81.93(17)° to 98.76(17)°. The equatorial Dy-O bonds to the coordinated THF ligands and the BQ ligand are in the range 2.388(6)–2.427(6) Å and 2.329(6)–2.338(6) Å, respectively. The latter bonds are slightly shorter, most likely due to the stronger electrostatic bonding. The Cl1 and Cl2 ligands are axially coordinated to dysprosium, with Dy-Cl distance of 2.603(2) Å and 2.587(2) Å, respectively. The shortest intermolecular distance between two Dy^{3+} ions is 7.7950(8) Å and the intramolecular distance between Dy1 and Dy2 is 8.5531(8) Å. Compound **1** shows very similar geometrical parameters to **2** (Figure S2 and Table S1).

Comparison of the powder X-ray diffraction patterns of **1** and **2** measured at 120 K to 293 K reveals that both structures undergo a significant anisotropic thermal expansion. Anisotropic expansion of the unit cells on both **1** and **2** are best seen along the b-axis, which elongates by almost 9% (the *b*-axis changes from 14.88 to 16.15 Å, and 15.00 to 16.15 Å for 1 and 2, respectively). In comparison, the *a*- and *c*-axes show 1-2% expansion. This expansion is evidenced also in unit cell volumes that increase from ~1900 to ~2050 Å3. To visualize the unit cell transformation and thermal expansion, the overlay of the packing of the low (120 K) and high (293 K) temperature crystal structures are shown in Figures 1c and S2. Both figures clearly show the elongation of intermolecular distance between complexes along b-axis of crystal structures. Due to the substantial changes in the unit cell parameters of **1** and **2**, their calculated diffraction patterns at 120 K differed when

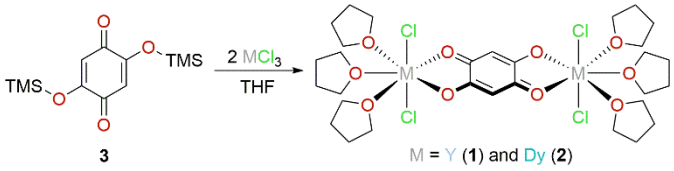

3

Scheme 1 The synthesis of **1** and **2**.

preliminary comparisons were made with powder diffraction data recorded at 293 K (Figure 2, Figure S3 and Figure S4). When additional single crystal data was acquired at 293 K, we were able to show that the room temperature single crystal data is actually identical with the measured powder diffraction data at 293 K as shown in Figure 2 for **2** and in Figure S3 for **1**. This confirms that the bulk powders and single crystals are structurally consistent with each other. The thermal expansion in complexes **1** and **2** presumably originates from the herringbone arrangement of the complexes in which each discrete complex interacts with neighbouring complexes mainly through weak dispersion force that can be modulated via thermal energy (Figure 1c, Figure S1, Figure S2 and Table S2). A similar type of thermal expansion has been observed for framework materials in which metallophilic interactions ($M^{+}\cdots M^{+}$) (M = Cu, Ag, Au) are largely responsible for the thermal expansions of the materials.[22]

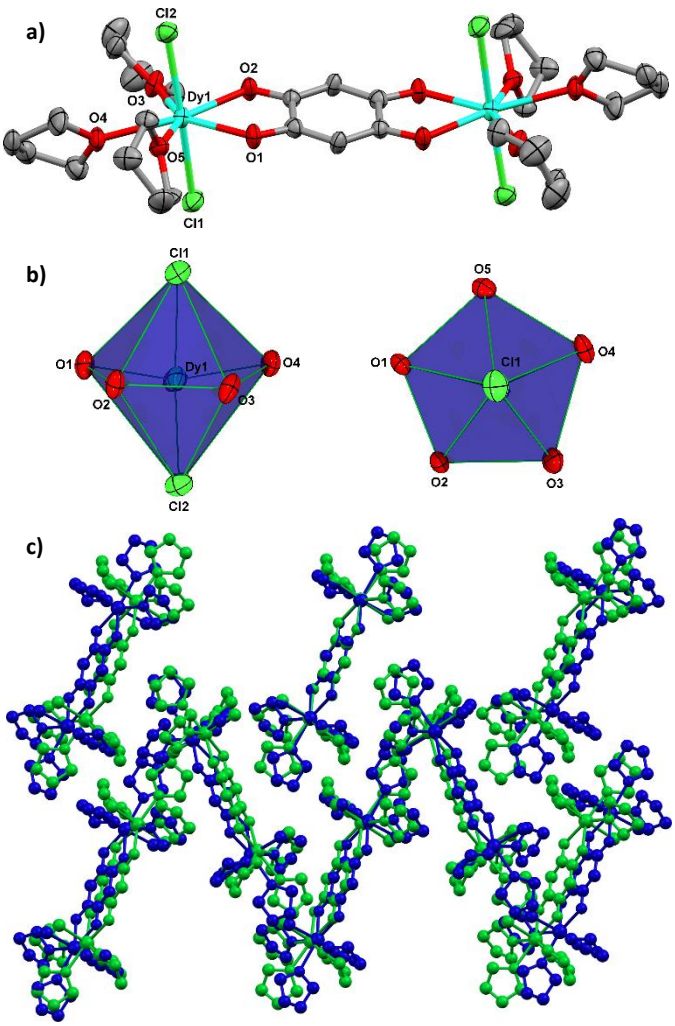

Figure 1 (a) Crystal structure of **2**. Thermal ellipsoids are drawn at 50% probability level and hydrogen atoms are omitted for clarity (black = C; red = O; Green = chlorine; turquoise = dysprosium). (b) The pentagonal bipyramidal environment around Dy^{3+} ions illustrated by polyhedra; side view (left) and top view (right). (c) The overlay picture of low (120 K, green) and high (293 K, blue) temperature structures along a-axis. Selected bond lengths and angles are given in Table S1.

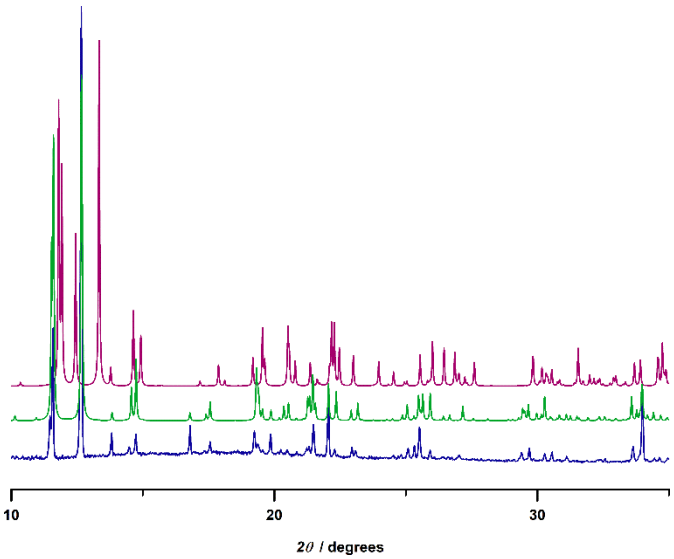

Figure 2 Calculated (red 120 K and green 293 K) and measured (blue 293 K) powder patterns from 10° to 35° for **2**. The full pattern (from 5° to 70°) and the data for **1** is given in supporting info (Figure S3 and S4).

The electrochemical properties of complexes **1** and **2** were studied by cyclic voltammetry (CV) using a Pt electrode and [(*n*-Bu)$_4$N]$^+$[PF$_6$]$^-$ as a supporting electrolyte in THF solutions. Both complexes showed one irreversible reduction process with similar $E^{1/2}$ values of -0.21 V and -0.21 V vs SCE for **1** and **2**, respectively (Figure 3).[‡] The result indicates that the nature of the rare earth ion has a very little effect on the observed reduction potential of the bridging ligand. This finding is in a good agreement with previous cyclic voltammetry studies carried out on redox-active bridged dinuclear rare-earth complexes.[9a] Interestingly, no other reduction processes were observed within the accessible redox window of the solvent for **1** and **2**, although it is known that the transition metal complexes of [BQ^{2-}] ligand can be reduced sequentially in two separate, one electron redox processes to a radical trianion [BQ3$^{\bullet-}$] and then to the tetraanion [BQ^{4-}].[1] While we cannot unambiguously assign the observed -1/0 wave of **1** and **2** at -0.21 V vs SCE to a one electron reduction processes from the CV results, the chemical reduction studies of **1** and **2** afforded complexes which contained the radical trianion [BQ$^{3\bullet-}$] (see below).

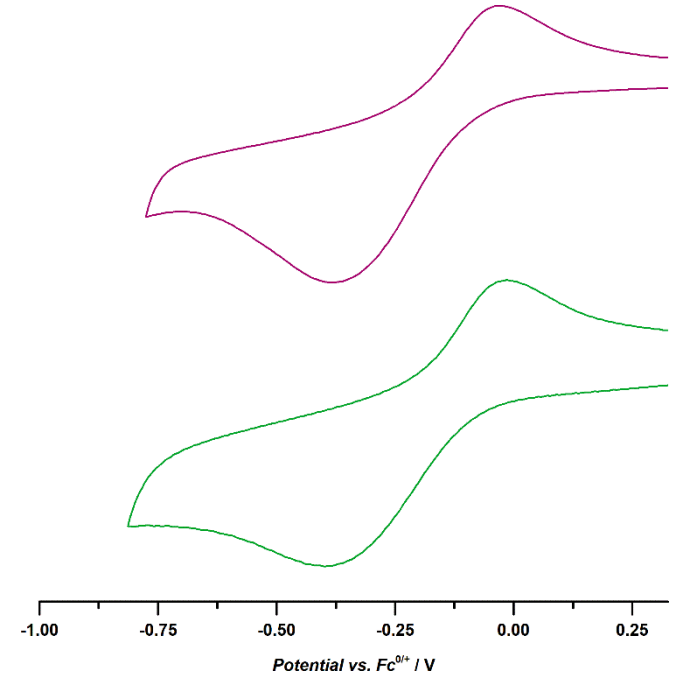

Figure 3 Cyclic voltammograms for **1** (red) and **2** (green) in THF solutions containing 0.1 M [(n-Bu)$_4$N]$^+$[PF$_6$]$^-$ at Pt electrode with scan rate 200 mV s^{-1}. Peak potentials and currents are given in Table S3.

In addition to CV measurements, the electron acceptor ability of the complexes was tested by reacting **1** and **2** with *tetrakis*(dimethylamino)ethylene (TDAE), in THF. During the reduction, a clear colour change occurred: an initially red suspension turned to a green solid. Evidence for the formation of a radical anion were acquired by performing X-band EPR spectroscopy on the powdered sample of the reduced complex **1**$^{\bullet-}$. As shown in Figure S5, the EPR spectrum of **1**$^{\bullet-}$ displays an intensive single peak with g_{iso} value of 2.003 G, which is typical for an organic radical with a doublet ground state. Moreover, a new absorption band of C=O stretch (≈ 1470 and **2**$^{\bullet-}$ indicating the formation of trianion [BQ$^{3\bullet-}$] as shown by previous studies (Figure S6 and Figure S7).[2a,c,23] Unfortunately, both reduced complexes were completely insoluble in all common organic solvents, which prevented characterization of their solid-state structures by single-crystal X-ray diffraction. However, the spectroscopic evidence and cyclic voltammetry measurements clearly demonstrate the redox activity of complexes **1** and **2**.

Variable-temperature DC magnetic susceptibility measurement was performed on a microcrystalline sample of 2 in a field of H = 1 T and in the temperature range 2-300 K. The measured room-temperature $\chi_M T$ value of 28.47 cm^3 K mol^{-1} is in good agreement with the theoretical value of 28.34 cm^3 K mol^{-1} for two non-interacting Dy^{3+} ions ($^6H_{15/2}$, g = 4/3). Upon cooling, $\chi_M T$ slowly decreases down to 25 K, and then rapidly reaches the minimum value of 10.41 cm^3 K mol^{-1} at 2 K (Figure

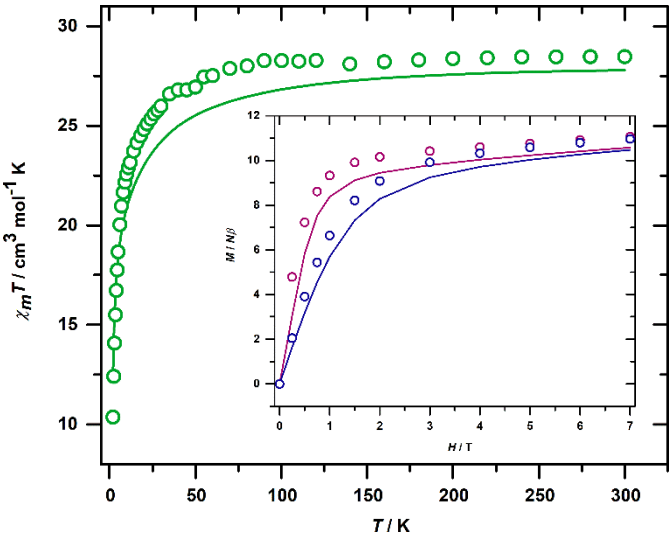

Figure 4 Experimental (green circles) and calculated (green solid line) plot of $\chi_M T$ as function of temperature in the field 1 T. Plots of M as function of magnetic field at 1.8 K (red) and 5 K (blue) (inset, dots = experimental data, solid lines = calculated data).

4). The inset of Figure 3 shows isothermal magnetization (M vs. H) plot for 2 at 2 K and 5 K. At both temperatures, the magnetization quickly increases to 2.0 T, and then rises gradually to the saturation value of 11.06 μ_B at 7 T.

Precise control of the local pseudo-D_{5d} crystal field symmetry around lanthanide metal centres has also been applied to design single-ion dysprosium complexes that function as single-molecule magnets (SMMs).[24] The strong magnetic anisotropy of Dy^{3+} ion in axial environments is enhanced by crystal fields with strong negatively charged axial donors but weakly charged equatorial donors. For example, $[Dy\text{-}(Cy_3PO)_2(H_2O)_5]Br_3\cdot 2(Cy_3PO)\cdot 2H_2O\cdot 2EtOH$ (Cy_3PO = tricyclohexyl phosphine oxide) complex displays open hysteresis loops up to 20 K[24e] and $[Dy(OtBu)_2(pyridine)_5][BPh_4]$ shows the second highest effective barrier for thermally activated relaxation of magnetization ever reported.[24d] Thus, we were interested to see if complex **2** and its diluted analogue **Dy@1** would display SMM behaviour. AC magnetic susceptibility measurements in zero dc field did not show any evidence of slow relaxation of the magnetization neither for **2** nor for **Dy@1**. To better understand this lack of SMM behaviour, quantum chemical calculations were carried out for **2**.

Ab initio calculations at CASSCF/SO-RASSI level (see computational details) show that the principal magnetic axes of the Dy^{3+} ions in **2** are not coincident with the pseudo-C_5 axes of the pentagonal bipyramidal coordination spheres, but are in fact rotated some 90° and lie in the molecular plane (Figure 5). This leads to non-negligible transverse components in the g tensor of the ground Kramers doublet (Table S4), which enables fast quantum tunnelling of magnetization (QTM). Rotation of the principal magnetic axes demonstrates that, although from a purely geometric point of view the ions have pentagonal bipyramidal coordination environments, the O-donor atoms of the $[BQ]^{2-}$ ligand provides a stronger, equatorial crystal field than the THF ligands or the Cl ions. Thus, from a magnetic point of view, the coordination environment has pseudo-C_{2v} symmetry with the principal axis in the molecular plane.

In principle, the ground state QTM could be supressed by sufficiently strong exchange interaction between the Dy^{3+} ions. SMM behaviour has indeed been observed in dinuclear dysprosium complexes which have similar coordination spheres around the Dy^{3+} as in **2**, that is, Cl and O atoms occupying the axial and equatorial sites of Dy^{3+} ions, respectively.[7] In these systems the ground state QTM is suppressed by relatively strong exchange interaction between the Dy^{3+} ions, with exchange parameter magnitudes of the order 3–7 cm^{-1} acquired by the Lines model.[7a,b] Therefore, following the Lines model, an effective intramolecular exchange parameter was determined for **2** by fitting an ab initio calculated susceptibility to the experimental data (see computational details). Owing to the large distance between the Dy^{3+} ions, the exchange parameter is weak (J = –0.142 cm^{-1}) and, thus, the exchange interaction is not strong enough to block the QTM process. It should be noted that the agreement between the experimental and calculated susceptibility and isothermal magnetization plots are not perfect (Figure 4). The deviations from experiment most likely arise from the electron correlation outside the 4f orbital space, which has been neglected in the CASSCF calculations. This correlation affects the crystal-field splitting of the Dy^{3+} ground $^6H_{15/2}$ multiplet and, consequently, influences the rate of thermal depopulation of excited levels as the temperature is lowered as well as the degree of mixing of states due to the Zeeman interaction.[25]

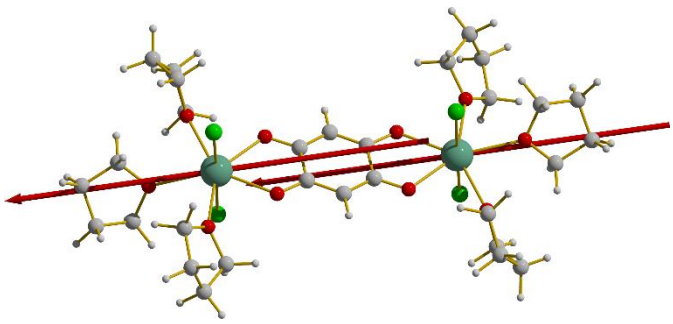

Figure 5 The principal magnetic axis of the ground Kramers doublet (red) of the two Dy^{3+} ions in **2**.

Conclusions

In conclusions, we have reported the synthesis of two discrete benzoquinone-bridged dinuclear rare-earth complexes $[BQ(MCl_2\cdot THF_3)_2]$ **1** and **2** (M = Y (**1**), Dy (**2**), BQ = 2,5-bisoxide-1,4-benzoquinone) in which the rare earth ions reside in pentagonal bipyramidal environments. The complexes are redox active as shown by cyclic voltammetry studies and the reduction of complexes with TDAE and subsequent characterization of **1** by EPR spectroscopy. The neutral complexes also undergo significant anisotropic thermal expansion when heated from 120 K to 293 K. AC magnetic susceptibility measurements revealed that complex **2** does not show any slow relaxation of the magnetization. The lack of SMM behaviour results from the rotation of the principal magnetic axis as compared to the pseudo-C_5 axis of the pentagonal bipyramidal environment, and from the lack of sufficiently strong intramolecular exchange interaction to block the ground state QTM, as shown by quantum chemical calculations. It should be possible to modulate the crystal field of complex **2** by substituting stronger and weaker donor atoms to axial and equatorial positions, respectively, as well as increase the solubility of the reduced species by introducing either alkyl or aryl substituents to the ligand framework. Thus, **2** can be considered to be a blueprint compound for bridged redox active multinuclear lanthanide SMMs that adhere to an SMM design criteria *i.e.* an ideal geometry coupled with bridging organic radical ligand.[24d]

Conflicts of interest

There are no conflicts to declare.

Acknowledgements

JOM, AM, ML and EK thank Academy of Finland (project numbers 285855 (JM), 282499 (AM), 277250 (ML), 284562 and 278743 (EK)), FSG thanks EC for an MSC Fellowship and RAL thanks the ERC for the Consolidator Grant 'RadMag'. Prof. H. M. Tuononen (University of Jyväskylä) is acknowledged by providing computational resources for the project. We also thank Laboratory Technician Elina Hautakangas (University of Jyväskylä) and Dr. Siiri Perämäki for elemental analyses and ICP measurements, respectively.

Notes and references

‡ In addition to the -1/0 reduction wave, one irreversible oxidation process was observed for both complexes (Table S3 and Figure S8).

1 S. Kitagawa and S. Kawata, *Coord. Chem. Rev*., 2002, **224**, 11.
2 For some examples, see: (a) K. S. Min, A. G. DiPasquale, A. L. Rheingold, H. S. White and J. S. Miller, *J. Am. Chem. Soc*., 2009, **131**, 6229. (b) C. Carbonera, A. Dei, J.-F. Létard, C. Sangregorio and L. Sorace, *Angew. Chem. Int. Ed.* 2004, **43**, 3135. (c) J. Tao, H. Maruyama and O. Sato, *J. Am. Chem. Soc*. 2006, **128**, 1790. (d) W. Cao, X. Zhu, P. Liu, S. Su, S. Hu, Y. Wen, X. Wua and T. Sheng, *Dalton Trans*., 2017, **46**, 3435.
3 (a) I.-R. Jeon, B. Negru, R. P. Van Duyne and T. D. Harris, *J. Am. Chem. Soc.*, 2015, **137**, 15699. (b) L. E. Darago, M. L. Aubrey, C. J. Yu, M. I. Gonzalez and J. R. Long, *J. Am. Chem. Soc*., 2015, **137**, 15703.
4 B. Therrien, G. Süss-Fink, P. Govindaswamy, A. K. Renfrew and P. J. Dyson, *Angew. Chem. Int. Ed.*, 2008, **120**, 3833.
5 (a) M. A. Subhan, R. Kawahata, H. Nakata, A. Fuyuhiro, T. Tsukuda and S. Kaizaki, *Inorg. Chim. Acta*, 2004, **357**, 3159. (b) B. F. Abrahams, J. Coleiro, K. Ha, B. F. Hoskins, S. D. Orchard, R. Robson, J. Chem. Soc. Dalton Trans., 2002, 1586.
6 (a) P. E. Riley, S. F. Haddad and K. N. Raymond, *Inorg. Chem*., 1983, **22**, 3090. (b) C. Robl, *Mater. Res. Bull*., 1987, **22**, 1483. (c) G. Zucchi, P. Thuery and M. Ephritikhine, *CSD Communication (Private Communication)*, 2012. (d) K. Nakabayashi and S. Ohkoshi, *Acta Cryst*., 2010, **E66**, m1300. (e) B. F. Abrahams, J. Coleiro, B. F. Hoskins and R. Robson, *Chem. Commun*., 1996, 603. (f) T. Demars, M. Boltoeva, N. Vigier, J. Maynadié, J. Ravaux, C. Genre and D. Meyer, *Eur. J. Inorg. Chem*., 2012, 3875. (g) K. Nakabayashi and S. Ohkoshi, *Inorg. Chem*., 2009, **48**, 8647.
7 (a) Y.-N. Guo, G.-F. Xu, W. Wernsdorfer, L. Ungur, Y. Guo, J. Tang, H.-J. Zhang, L. F. Chibotaru and A. K. Powell, *J. Am. Chem. Soc*., 2011, **133**, 11948. (b) Q. Chen, F. Ma, Y.-S. Meng, H.-L. Sun, Y.-Q. Zhang and S. Gao, *Inorg. Chem*., 2016, **55**, 12904. (c) Y. Jiang, G. Brunet, R. J. Holmberg, F. Habib, I. Korobkov and M. Murugesu, *Dalton Trans*., 2016, **45**, 16709. (d) D. N. Woodruff, R. E. P. Winpenny and R. A. Layfield, *Chem. Rev*. 2013, **113**, 5110. (e) R. A. Layfield, *Organometallics*, 2014, **33**, 1084.
8 (a) X.-C. Huang, M. Zhang, D. Wu, D. Shao, X.-H. Zhao, W. Huanga and X.-Y. Wang, *Dalton Trans*., 2015, **44**, 20834. (b) G.-J. Zhou, Y.-S. Ding and Y.-Z. Zheng, *Dalton Trans*., 2017, **46**, 3100. (c) S. She, B. Liu, Y. Yang, Z. Ba, L. Gong, B. Wang and S. Min, *Inorg. Chem. Commun*., 2015, **61**, 132.
9 (a) S. Demir, M. Nippe, M. I. Gonzaleza and J. R. Long, *Chem. Sci*., 2014, **5**, 4701. (b) F.-S. Guo and R. A. Layfield, *Chem. Commun*., 2017, **53**, 3130. (c) B. S. Dolinar, S. Gómez-Coca, D. I. Alexandropoulos and K. R. Dunbar, *Chem. Commun*., 2017, **53**, 2283. (d) S. Demir, J. M. Zadrozny, M. Nippe and J. R. Long, *J. Am. Chem. Soc*., 2012, **134**, 18546.
10 CrysalisPro program, version 1.71.38.43, Agilent Technologies, Oxford, 2012.
11 G. M. Sheldrick, *Acta Cryst*. 2008, **A64**, 112.
12 G. M. Sheldrick, *Acta Cryst*. 2015, **C71**, 3.
13 O.V. Dolomanov, L. J. Bourhis, R. J. Gildea, J. A. K. Howard and H. Puschmann, *J. Appl. Cryst*, 2009, **42**, 339.
14 F. Aquilante, J. Autschbach, R. K. Carlson, L. F. Chibotaru, M. G. Delcey, L. De Vico, I. Fdez. Galván, N. Ferré, L. M. Frutos, L. Gagliardi, M. Garavelli, A. Giussani, C. E. Hoyer, G. Li Manni, H. Lischka, D. Ma, P. Å. Malmqvist, T. Müller, A. Nenov, M. Olivucci, T. B. Pedersen, D. Peng, F. Plasser, B. Pritchard, M. Reiher, I. Rivalta, I. Schapiro, J. Segarra-Martí, M. Stenrup, D. G. Truhlar, L. Ungur, A. Valentini, S. Vancoillie, V. Veryazov, V. P. Vysotskiy, O. Weingart, F. Zapata and R. Lindh, *J. Comp. Chem*., 2016, **37**, 506.
15 (a) K. Andersson, P. Å. Malmqvist and B. O. Roos, *J. Chem. Phys.,* 1992, **96**, 1218. (b) B. O. Roos, R. Lindh, P. Å. Malmqvist, V. Veryazov, and P.-O. Widmark, *J. Phys. Chem. A*, 2004, **108**, 2851. (c) B. O. Roos, R. Lindh, P. Å. Malmqvist, V. Veryazov, P.-O. Widmark and A. C. Borin, J. *Chem. Phys. A*, 2008, **112**, 11431.
16 (a) W. Kutzelnigg and W. Liu, *J. Chem. Phys*., 2005, **123**, 241102. (b) M. Filatov, *J. Chem. Phys*., 2006, **125**, 107101. (c) P. Daoling and M. Reiher, *Theor. Chem. Acc*., 2012, **131**, 1.
17 (a) B. O. Roos, *The Complete Active Space Self-Consistent Field Method and Its Applications in Electronic Structure Calculations in Advances in Chemical Physics: Ab Initio Methods in Quantum Chemistry II*, Vol. 69, K. P. Lawley (Ed.), Wiley, New York, 1987, 399–455. (b) B. O. Roos, R. Lindh, P. Å. Malmqvist, V. Veryazov and P.-O. Widmark, *Multiconfigurational Quantum Chemistry*, Wiley, Hoboken, 2016.
18 P. Å. Malmqvist, B. O. Roos and B. Schimmelpfennig, *Chem. Phys. Lett*., 2002, **357**, 230.
19 L. F. Chibotaru and L. Ungur, *J. Chem. Phys*., 2012, **137**, 064112.
20 (a) L. F. Chibotaru, L. Ungur and A. Soncini, *Angew. Chem. Int. Ed*., 2008, **47**, 4126. (b) L. Ungur, W. Van den Heuvel and L. F. Chibotaru, *New. J. Chem*., 2009, **33**, 1224.
21 M. E. Lines, *J. Chem. Phys*., 1971, **55**, 2977.
22 (a) A. L. Goodwin, Ma. Calleja, M. J. Conterio, M. T. Dove, J. S. O. Evans, D. A. Keen, L. Peters and M. G. Tucker, *Science*, 2008, **319**, 794. (b) J. L. Korčok, M. J. Katz and D. B. Leznoff, *J. Am. Chem. Soc*. 2009, **131**, 4866. (c) J. S. Ovens and D. B. Leznoff, Inorg. Chem., article ASAP, DOI:10.1021/acs.inorgchem.6b03153
23 K. S. Min, A. G. DiPasquale, J. A. Golen, A. L. Rheingold and J. S. Miller, *J. Am.* Chem. *Soc*., 2007, **129** , 2360.
24 (a) J.-L. Liu, Y.-C. Chen, Y.-Z. Zheng, W.-Q. Lin, L. U., W. Wernsdorfer, L. F. Chibotaru and M.-L. Tong, *Chem. Sci*., 2013, **4**, 3310. (b) S. K. Gupta, T. Rajeshkumar, G Rajaraman and R. Murugavel, *Chem. Sci*., 2016, **7**, 5181. (c) J. Liu, Y.-C. Chen, J.-L. Liu, V. Vieru, L. Ungur, J.-H. Jia, L. F. Chibotaru, Y. Lan, W. Wernsdorfer, S. Gao, X.-M. Chen and M.-L. Tong, *J. Am. Chem. Soc*. 2016, **138**, 5441. (d) Y.-S. Ding, N. F. Chilton, R. P. Winpenny and Y.-Z. Zheng, *Angew.Chem. Int.Ed*., 2016, **55**, 16071. (e) Y.-C. Chen, J.-L. Liu, L. Ungur, J. Liu, Q.-W. Li, L.-F. Wang, Z.-P. Ni, L. F. Chibotaru, X.-M. Chen, M.-L. Tong, *J. Am. Chem. Soc*. 2016, **138**, 2829. (f) Y.-C. Chen, J.-L. Liu, Y. Lan, Z.-Q. Zhong, A. Mansikkamäki, L. Ungur, Q.-W. Li, J. -H. Jia, L. F. Chibotaru, J. -B. Han, W. Wernsdorfer, X.-M. Chen and M.-L. Tong, *Chem. Eur. J*., 2017, **23**, 1.
25 L. Ungur and L. F. Chibotaru, *Chem. Eur. J*. 2017, **23**, 3708.